

PAPER • OPEN ACCESS

## Investigation on Microstructure and Mechanical Properties of Continuous and Pulsed Current Gas Tungsten Arc Welded alloy 600

To cite this article: A Srikanth and M Manikandan 2018 *IOP Conf. Ser.: Mater. Sci. Eng.* **310** 012073

View the [article online](#) for updates and enhancements.

# Investigation on Microstructure and Mechanical Properties of Continuous and Pulsed Current Gas Tungsten Arc Welded alloy 600

Srikanth A<sup>1</sup>, Manikandan M<sup>1\*</sup>

<sup>1</sup>School of Mechanical Engineering, VIT University, Vellore, India

\*E-mail: mano.manikandan@gmail.com

**Abstract.** The present study investigates the microstructure and mechanical properties of joints fabricated by Continuous and pulsed current gas tungsten arc welded alloy 600. Welding was done by autogenous mode. The macro examination was carried out to evaluate the welding defects in the weld joints. Optical and Scanning Electron Microscope (SEM) were performed to assess the microstructural changes in the fusion zone. Energy Dispersive Spectroscopy (EDS) analysis was carried to evaluate the microsegregation of alloying elements in the fusion zone. The tensile test was conducted to assess the strength of the weld joints. The results show that no welding defects were observed in the fusion zones of Continuous and Pulsed current Gas Tungsten Arc Welding. The refined microstructure was found in the pulsed current compared to continuous current mode. Microsegregation was not noticed in the weld grain boundary of continuous and pulsed current mode. The pulsed current shows improved mechanical properties compared to the continuous current mode.

**Keyword:** Alloy 600, Pulsed Current Gas Tungsten Arc welding, Microstructure, Microsegregation

## 1. Introduction

Alloy 600 is a single phase solid solution strengthened nickel-based super alloy. The major alloying elements are Cr and Fe along with minor alloying additives. There is no precipitation strengthening involving in this alloy [1]. The alloy is widely used in the high-temperature environment. For example steam generator tubing, control rod drive and pressurized nozzles in nuclear power plant due to excellent resistance to corrosion and oxidation [2]. It is a workhorse material for the construction of nuclear reactors. The alloy 600 has led to use a variety of applications involving temperature from cryogenic to above 1095 °C [1].

Welding plays an inevitable role in a broad range of above-said applications. Arc welding is the commonly used welding technique in the industry and also the cost effective process compared to the other welding process. Welding of this alloy is possible by GTAW or GMAW processes. Fusion welding resulted in some problems in this alloy [3-5]. The resistance of alloy 600 weldments to intergranular corrosion, on the other hand, received limited attention. The microsegregation that occurs in the weld fusion zone of alloy 600 leads to the situation where the grain boundary regions are impoverishment or depletion of chromium [6]. The segregation within the matrix and grain boundary results in reducing the corrosion resistance of the weld joint as compared to the base metal.



The clue to prevent the intergranular corrosion hence lies lessen the microsegregation of Cr. This can be mitigated by control of the weld metal composition and temperature during welding [7]. Shimada et al. [8]. reported that alloy 600 had shown highly prone to sensitization and very high susceptibility to intergranular corrosion even in as-received annealed condition. Sato et al. [7] studied the microstructure properties of friction stir welded alloy 600. The authors observed the fine grain structure in the stir zone and improved mechanical properties than the base metal. The stir zone and HAZ exhibited a minor corrosion resistance than the base metal. Yun soo et al. [9] examine the microstructure of alloy 600/182 weld. The matrix of alloy 600 was identified as  $Cr_7C_3$  irrespective of the intergranular and intragranular ones. The authors observed that  $M_{23}C_6$  and Nb carbides were distributed on the grain boundaries in the weld metal. Gorman et al. [10] reported that the alloy 600 has been prone to stress corrosion cracking in the primary waterside environments. The susceptibility of interdendritic stress corrosion cracking is influenced by the grain boundary chemistry/structure, secondary phases precipitation and other metallurgical factor. [11-16].

Based on the previous literature the microsegregation of Cr leads to the intergranular corrosion in the alloy 600 weldment. This can be brought down by controlled heat input during the welding process. Some literature promised that the same in other Ni-based superalloys. Manikandan et al. [17 & 18] evaluate the microsegregation of alloying elements in the alloy C-276 fabricated by GTA and PCGTA welding technique. The authors found that PCGTA obtained reduced microsegregation compared to GTAW. Similarly, Janaki Ram et al. [19] compared the laves phases formation of weld joints produced by GTA and PCGTA welding technique. The authors observed the PCGTAW shows the reduced volume percent of laves phases formation compared to GTAW.

As evident from the literature hitherto there is no research work reported on the welding of alloy 600 by GTAW and PCGTAW. The present research work addresses the effect of microsegregation of alloying elements in alloy 600 when switch over from GTAW to PCGTAW. The outcome of the results obtained in the present research work will be highly benefits in the nuclear industries where the material is employed for the fabrication process.

## 2. EXPERIMENTAL PROCEDURE

Alloy 600 was procured in the form of 4 mm solution annealed thick plate. The chemical composition of the as received plate is given in Table 1.

**Table 1.** The chemical composition of the base metal.

Base Metal	Chemical Composition (% Wt.)							
	Ni	Cr	Fe	Mn	Si	C	Cu	S
Alloy 600	77.70	15.42	6.181	0.334	0.306	0.041	0.010	0.008

The weld coupons were prepared with the dimensions of 55 X 130 X 4 mm. Plates were cleaned with acetone to remove the dirt around the edges. Welding trials were carried out, and the optimized process parameters are listed in Table 2.

**Table 2.** Process parameters

Welding Process	Current (A)	Voltage (V)	Welding Speed (mm/sec.)	Heat Input (j/mm)	Total Heat Input (j/mm)
GTA Autogenous	150	13.9	1.81	806.35	1746.56
	150	14.5	1.81	841.16	
PCGTA Autogenous		12.5	1.11	886.82	1647.51
		11.9	1.09	859.74	

Welding was done using KEMPPII DWE manually machine with argon as shielding gas with a flow of 15 L/min. Welding was done on both sides of the plate to achieve the full depth of penetration. Figure 1 shows the photographs of weld joints fabricated by GTA and PCGTA welding process.

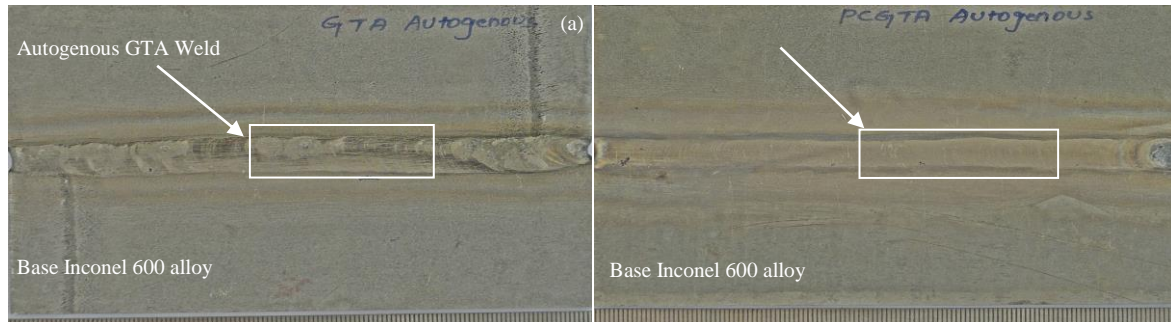


**Figure 1.** Photographs of weld joints (a) Autogenous GTA weld; (b) Autogenous PCGTA weld

Test coupons were extracted in the direction transverse to the welding direction. Standard procedure was applied to polish the specimen. To reveal the microstructure electrolytic etching was done in oxalic acid with 10 V DC power supply. Microstructure evaluates carried out to see the structural changes in the weld joints. SEM/EDS analysis was conducted to assess the microsegregation of alloying elements with emphasis to Ni, Cr, and Fe. Tensile test specimens were prepared as per the ASTM E8 standards to evaluate the strength of the weld joints. Stain rate of 2 mm/min was employed to perform the tensile test. Tensile test specimens were done triplicate to ensure the replicability of the results. SEM fractographic analysis was carried on the tensile failure specimen to evaluate the mode of failures.

### 3. Results and Discussions

#### 3.1 Macro Examination

The macro review of the weld joints produced by GTA and PCGTA are shown in Figure 2 (a and b). The macrograph shows the defect free welding was achieved in the process parameters employed in the present study. There is no problem in the lack of penetration and any other cracks in the fusion zone and HAZ. The width of the fusion zone in the PCGTA is less than the GTAW. The lower heat input employed in the PCGTAW is widely responsible for, the lesser width. In general, the higher heat input used in the nickel-based superalloy leads to cracking in the fusion zone [20]. Such cracks were not noticed in the present study. This confirmed that the process parameters used in the present studies are optimal.

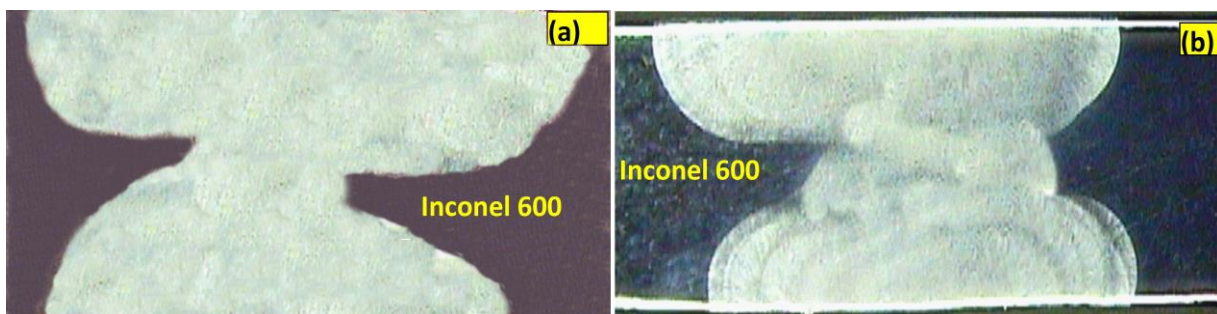


**Figure 2.** Macrostructure of Weld joints produced (a) Autogenous GTA weld (b) Autogenous PCGTA weld.

### 3.2 Microstructure Examination

The microstructure of as-received base metal alloy 600 is shown in fig. 3. The microstructure consists of austenite structure with well-defined grain boundaries. Solution annealing forms the annealing twins in many of the grain boundaries. The twin boundary avoids the dislocation motion and improves the strength of alloy 600.

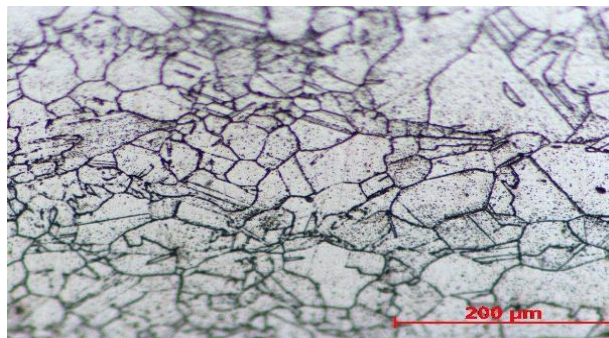


**Figure 3.** Microstructure of base metal alloy 600

The microstructure of the GTA and PCGTA welded alloy 600 is illustrated in Figs. 4 and 5. Figure 4a represents the fusion zone of the GTAW. The fusion center consists of cellular structure. Figure 5a represents the corresponding region of PCGTA. The fusion zone consists of the fine equiaxed dendritic structure. The weld interface areas both GTA and PCGTA show the formation of planar, and columnar dendritic structures. During the solidification, the mode changes from planar, cellular or dendritic in the case of GTAW and equiaxed dendritic in the case of PCGTA.

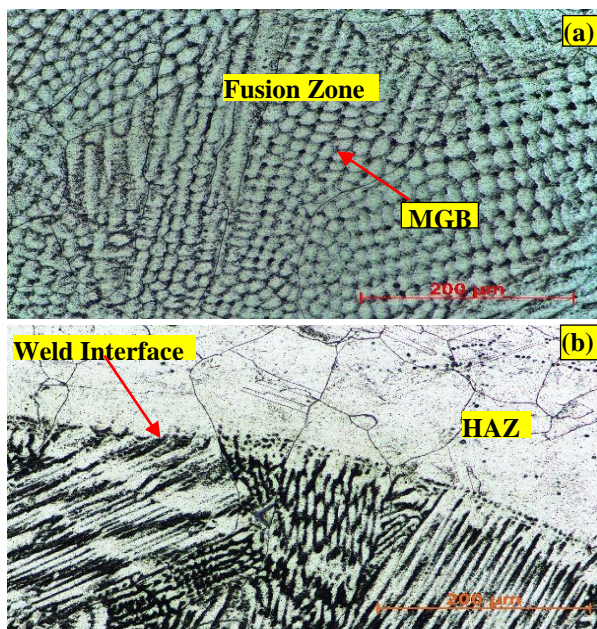


**Figure 4.** Microstructure of GTA welded alloy 600  
(a) Fusion zone and (b) Weld Interface

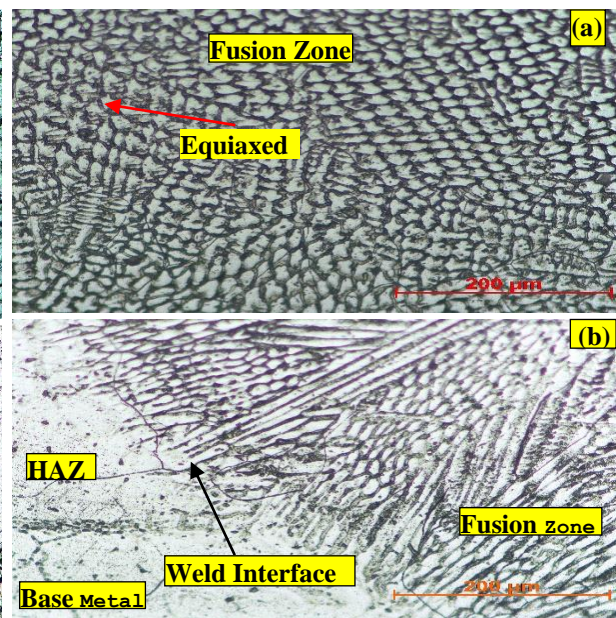


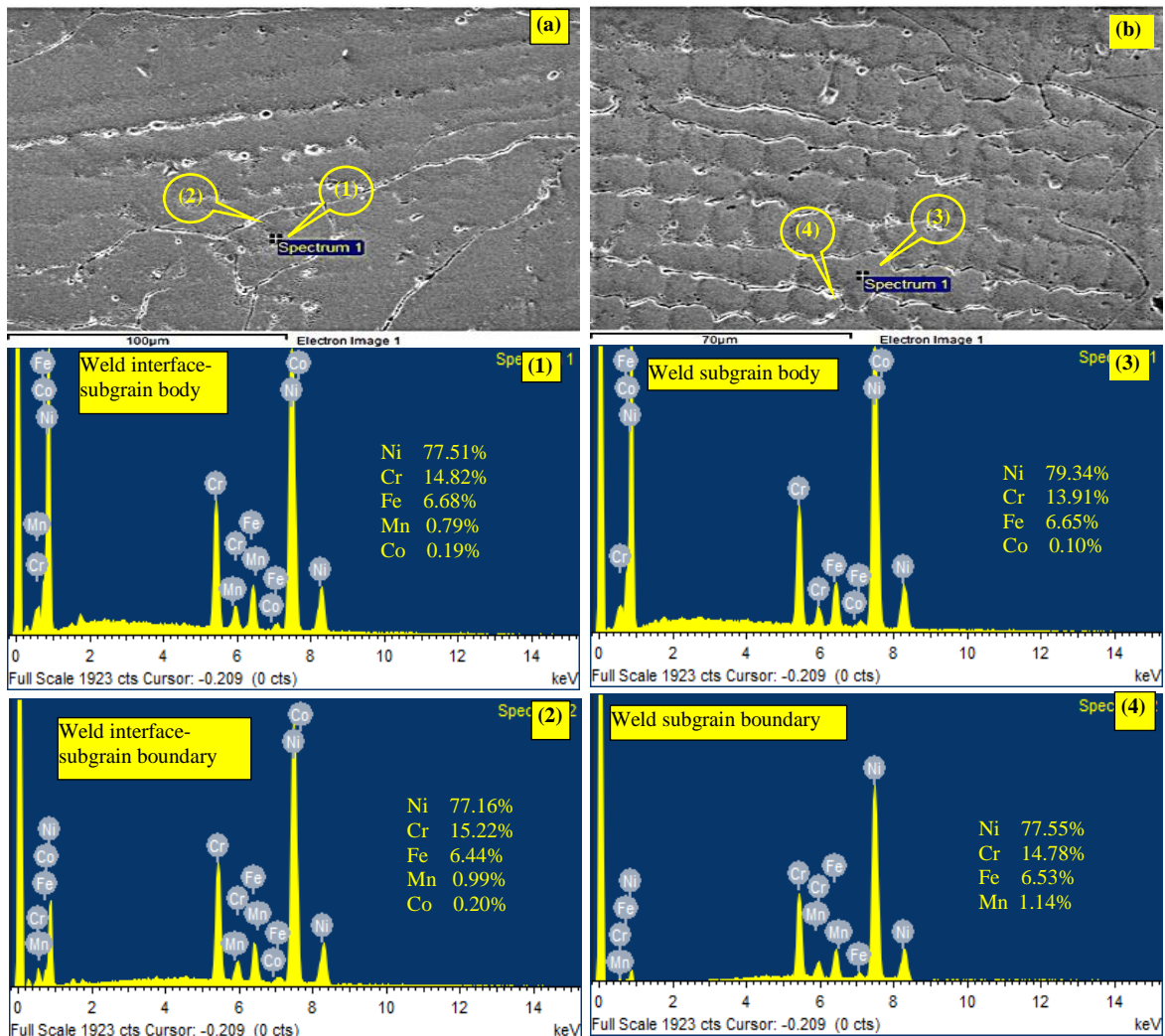
**Figure 5** Microstructure of PCGTA welded alloy 600 (a) Fusion zone and (b) Weld Interface

The mode of solidification depending on as the degree of constitutional supercooling continues to increase. The relative slower cooling rate in the GTAW will tend to have coarse cellular structure because the solid crystal phase forms at a temperature near the top of the melting range, where nucleation of many particles is difficult, but the growth of nucleated particles is easy because diffusion is enhanced at higher temperatures [21]. In contrast to GTA faster cooling in the PCGTA

weldments tends to produce relatively fine microstructure, because the alloy quickly solidifies with less diffusion-activated growth of the grains. A similar refinement of microstructure infusion zone was reported for alloy Inconel 617 and C-276 on switching over from GTAW to PCGTAW (Farahani et al. [22] & Manikandan et al. [17, 18, 23]). In both the cases, the migration grain boundaries were observed in the fusion zone. The solidification grain boundary results in a compositional gradient during the solidification.

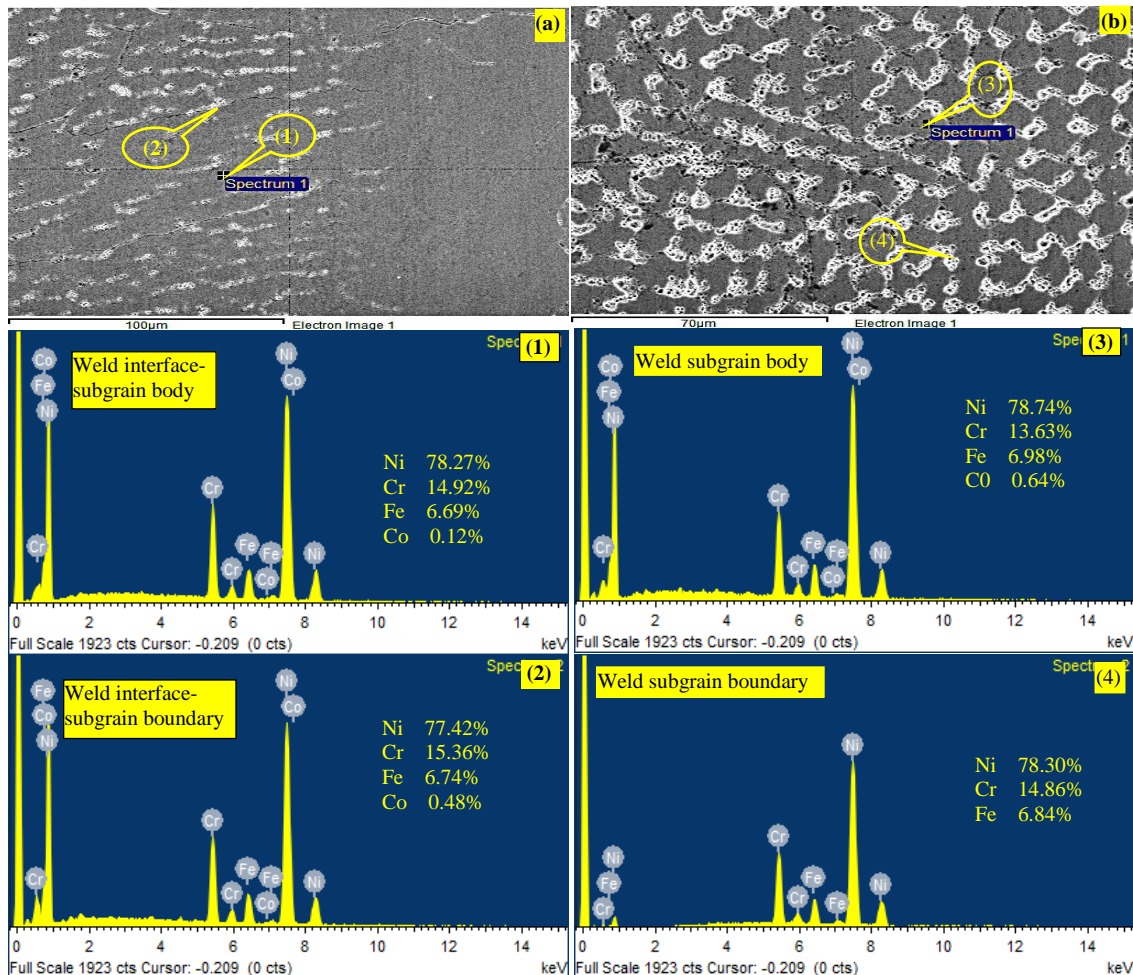
### 3.3SEM/EDS Analysis

Figure 6 and 7 representing the SEM/EDS analysis of GTA and PCGTA welded alloy 600. Figure 6 & 7 (a and b) represent the higher magnification SEM image of GTA and PCGTA. Figure 6a and 7a shows the weld interface regions. It consists of planar and columnar dendrite structure. Figure 6b and 7b represent the SEM image of weld center.



**Figure 6.** SEM/EDAX analysis of GTA welded alloy Inconel 600 for different region of the weldment. (a)SEM- Weld Interface; (b)SEM- Weld Centre; (1)Weld interface-subgrain body; (2)Weld interface-subgrain boundary; (3)Weld subgrain body; (4)Weld subgrain boundary.

The GTAW weldments show the cellular structure and the PCGTA show the equiaxed dendrite structure. The weld center and interface indicate the presence of Cr-rich  $M_{23}C_6$  carbide phases in the interdendritic regions. As pointed out in the Introduction section alloy 600 prone to hot cracking due to the microsegregation of Cr during solidification. EDS analysis was carried out to evaluate the microsegregation of alloying elements in the weld joints produced by GTA and PCGTA weldments. Emphasis was given to monitoring Ni, Cr, Fe, and Co. It is observed that the elements levels in the Cr are almost same in the grain boundary regions compared to the matrix in both weld interface and fusion zone center (fig 6-7 (i-iv)). In the present study, there is no direct evidence to confirm that the presence of  $M_{23}C_6$  carbide phases in the fusion zone. Further TEM and EPMA technique are require to confirm the presence. This will be taken up in the near future.



**Figure 7.** SEM/EDAX analysis of PCGTA welded alloy Inconel 600 for different region of the weldment. (a)SEM- Weld Interface; (b)SEM- Weld Centre; (1)Weld interface-subgrain body; (2)Weld interface-subgrain boundary; (3)Weld subgrain body; (4)Weld subgrain boundary.

### 3.4 Mechanical Property

Figure 8 illustrate the tensile failure photograph of GTA and PCGTA welded alloy 600. In both cases, the failure occurred in the base metal regions. GTAW and PCGTAW obtained 600 MPa and 595 MPa strength. The strength of the base metal was obtained at 590 MPa. The observed results show that the weld metals are stronger than the base metal. SEM fractography analysis (fig. 8(c & d)) was carried out to evaluate the mode of failure. In both cases, the micrograph shows the microvoids with elongated dimples. It confirmed the failures occurred in the ductile mode.

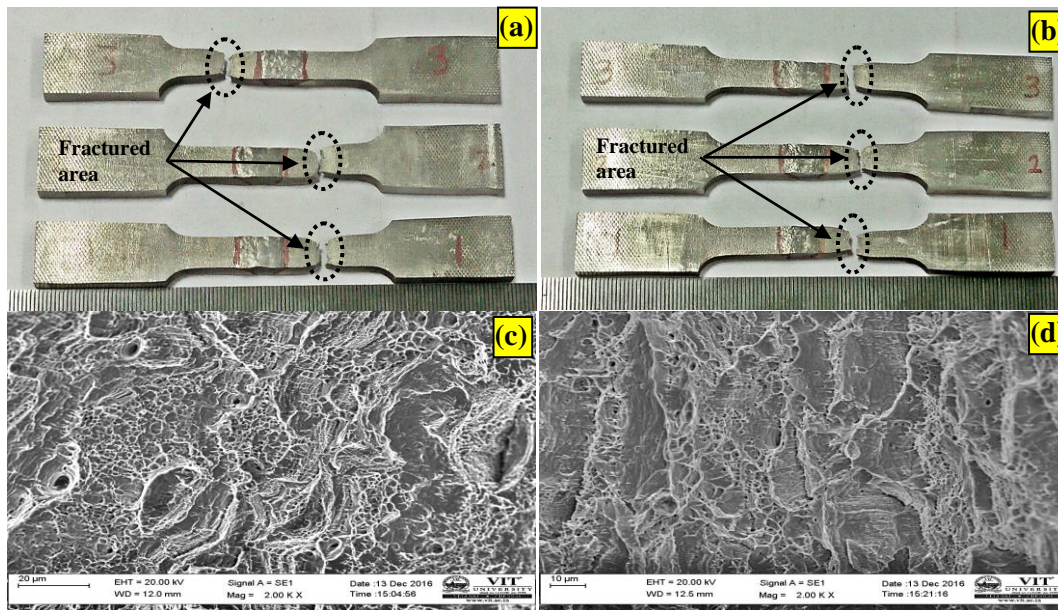


**Figure 8.** Photographs of fractured tensile tested specimens (a) Autogenous GTA weld; (b) Autogenous PCGTA weld; and SEM fractograph of the tensile tested specimens (c) Autogenous GTA weld; (d) Autogenous PCGTA weld

## 4. Conclusion

1. Defect free weld joints was obtained in the optimized process parameters
2. The lower heat input with faster cooling rate achieved in the PCGTAW shows the refined microstructure compared to GTAW
3. SEM/EDS analysis didn't provide the direct evidence for the presence of any secondary phases.
4. PCGTAW obtained improved mechanical properties compared to GTAW.

## 5. References

- [1] Webdata: <http://www.specialmetalswiggins.co.uk/pdfs/products/INCONEL%20alloy%20600.pdf>
- [2] Hur D H and Lee D H 2014 *Mater. Sci. Eng. A* **603** 129–133
- [3] Was G S and Kruger R M 1985 *Acta Metall* **33(5)** 841 – 854
- [4] Lim Y S, Kim H P, Han J H, Kim J S and Kwon H S 2001 *Corrosion Sci.* **43** 1321–1335
- [5] WS, Miami and FL 1996 *Welding Handbook 3* **8th ed.** 218-288
- [6] Sunil Kumar B, Prasad B S, Kain V and Reddy J 2013 *Corros. Sci.* **70** 55–61
- [7] Sato Y S, Arkom P, Kokawa H, Nelson T W and Steel R J 2008 *Mater. Sci. Eng. A* **477(1–2)** 250–258
- [8] Shimada M, Kokawa H, Wang Z, Sato Y and Karibe I 2002 *Acta Mater* **50** 2331-2341

- [9] Kim Y S, Maeng W Y and Kim S S 2015 *Acta Mater.* **83** 507–515
- [10] Gorman J, Hunt S and Riccardella P 2006 *ASME* **3** Chapter 44
- [11] Andresen P L 1996 *NACE* Paper #96258
- [12] Scott P M and Le Calvar M in: Proceedings of 6th International Symposium on Environmental Degradation of Materials in Nuclear Power Systems – Water Reactors, San Diego, CA, American Society for Metals, Materials Park, OH, 1993, p. 657.
- [13] Scott P M in: Proceedings of 9th International Symposium on Environmental Degradation of Materials in Nuclear Power Systems – Water Reactors, Newport Beach, CA, TMS, Warrendale, PA, 1999, p. 3.
- [14] Angeliu T M, Paraventi D J and Was G S 1995 *Corrosion* **51** 837
- [15] Onchi T, Dohi K, Soneda N, Navas M and Castano M L 2005 *J. Nucl. Mater.* **340** 219.
- [16] Scott P M 2013 presented at the *INL Seminar* on SCC in LWRs, Idaho Falls, Idaho p. **32**.
- [17] Manikandan M, Arivazhagan N, Rao M N and Reddy G M 2014 *J Manuf Process* **16** 563-572
- [18] Manikandan M, Arivazhagan N, Nageswara Rao M and Madhusudhan Reddy G 2014 *Acta Metall. Sin. (English Lett.)* **28(2)** 208–215
- [19] Janaki Ram G D, Venugopal Reddy A, Prasad Rao K, Reddy G M and Sarin Sundar J K 2005 *J. Mater. Process. Technol.* **167(1)** 73–82
- [20] John Dupoint N, John Lippold C and Samuel Kiser D *Welding metallurgy and weldability of nickel-base alloys*. 1st ed. USA: John Wiley & Sons, Inc.; 2009.
- [21] George F and Vander Voort 2004 *Metallography and Microstructures ASM Handbook* **9** ASM International, USA
- [22] Farahani E, Shamanian M and Ashrafizadeh F 2012 *AMAE Int J Manuf Mater Sci* **2(1)** 1–6
- [23] Arulmurugan B and Manikandan M. 2017 *Mater. Sci. Eng. A* **691** 126–140